Solid State Nuclear Magnetic Resonance 143 (2026) 102074

Contents lists available at ScienceDirect

Solid State Nuclear Magnetic Resonance

journal homepage: www.elsevier.com/locate/ssnmr

Investigation of the late-Roman burial chamber at Reichertsberg in Trier by NMR depth profiling

C. Golini [a], Q. Yang [b], M. Waldecker [b], R. Lenz [c], L. Brizi [a], S. Haber-Pohlmeier [d,e], A. Pohlmeier [d], P. Tomassini [f], J. Frick [e], J. Anders [b], B. Blümich [g,*], F. Heimerl [h]

[a] University of Bologna, Dipartimento di Fisica e Astronomia, Viale Berti Pichat 6/2, 40127 Bologna, Italy
[b] University of Stuttgart, Institute of Smart Sensors, Pfaffenwaldring 47, 70569 Stuttgart, Germany
[c] Staatliche Akademie der Bildenden Künste, Am Weißenhof 1, 70191, Stuttgart, Germany
[d] IGB-3, Forschungszentrum Jülich GmbH, Wilhelm-Johnen-Str., Jülich, 52428, Germany
[e] University of Stuttgart, Materialprüfungsanstalt, Pfaffenwaldring 2b, 70569, Stuttgart, Germany
[f] Université Catholique de Louvain, Histoire de L'art et Archéologie, Pl. de L'Université 1, 1348, Ottignies-Louvain-la-Neuve, Belgium
[g] RWTH Aachen University, Institut für Technische und Makromolekulare Chemie, Worringer Weg 2, 52074, Aachen, Germany
[h] University of Trier, Universitätsring 15, 54296, Trier, Germany

ARTICLE INFO

Handling Editor: Olivier Lafon

Keywords:
NMR relaxometry
NMR depth profiling
Mobile NMR
Cultural heritage
Plaster
Moisture flux
Diffusion

ABSTRACT

Trier is the oldest city in Germany with many relics of the Roman Empire. One of them is the burial chamber at Reichertsberg. Since its discovery in 1967 it has been excavated and secured with protecting outer walls. Located largely intact in a mountain slope at the back of a school yard it had been neglected until a detailed study 30 years later. In an effort to draw attention to its deteriorating state of preservation, the interior decorations were investigated in September 2025 along with NMR depth profiling of the plaster layers applied on three different occasions in the 3rd to 4th century AD. The NMR measurements are reported here along with an estimation of the moisture flux inside the plaster cover of a naturally wet inner wall.

1. Introduction

1.1. The burial chamber

Trier was founded as *Augusta Treverorum* in 18/17 BC and is considered the oldest city in Germany [1]. In late antiquity, Trier became one of the most important cities in the Roman West as an imperial residence and administrative center. During this time many important buildings were erected, the spectacular ruins of which are still visible today. A lesser-known site is the burial chamber in the mountain slope at Reichertsberg dating from the 3rd to 4th century AD (Fig. 1a) [2]. It was discovered during construction of the Reichertsberg elementary school in 1967 and since then is only accessible on demand. In antiquity, a staircase led down to the underground entrance of the chamber, which is now at ground level. The chamber probably had a temple-like superstructure that is no longer preserved. The interior of the chamber is almost square in shape $(3.6\ \mathrm{m})^2$, with a barrel vault ceiling reaching a maximum height of 2.84 m. Following its excavation and subsequent implementation of protective measures, the burial chamber has been in a state of negligence until the state of the burial chamber including its wall paintings and wall plasters were analyzed in detail in 1998 [3]. Four different building phases have been identified. These are in chronological order:

Phase 1 refers to the initial construction with a narrow corridor leading inside (Fig. 1b–A). Lower inside walls (Fig. 1b–B) formed three compartments (Fig. 1b, C–E), which were arranged like couches in a

This article is part of a special issue entitled: Reimer Special Issue published in Solid State Nuclear Magnetic Resonance.

* Corresponding author.
E-mail addresses: carlo.golini2@unibo.it (C. Golini), qing.yang@iis.uni-stuttgart.de (Q. Yang), maximiliane.waldecker@iis.uni-stuttgart.de (M. Waldecker), roland.lenz@abk-stuttgart.de (R. Lenz), leonardo.brizi2@unibo.it (L. Brizi), Sabina.Haber-Pohlmeier@mpa.uni-stuttgart.de (S. Haber-Pohlmeier), a.pohlmeier@fz-juelich.de (A. Pohlmeier), paolo.tomassini@uclouvain.be (P. Tomassini), juergen.frick@mpa.uni-stuttgart.de (J. Frick), jens.anders@iis.uni-stuttgart.de (J. Anders), bluemich@itmc.rwth-aachen.de (B. Blümich), heimerl@uni-trier.de (F. Heimerl).

https://doi.org/10.1016/j.ssnmr.2026.102074
Received 3 January 2026; Received in revised form 9 March 2026; Accepted 9 March 2026
Available online 19 March 2026
0926-2040/© 2026 The Authors. Published by Elsevier Inc. This is an open access article under the CC BY license (http://creativecommons.org/licenses/by/4.0/).

Roman dining room and served as a burial site for six individuals. Each compartment had a niche in the outer wall which may have served to light the chamber with oil lamps (Fig. 1b, niches I-III). The small brick walls (Fig. 1b–B) have a brownish base plaster, ca. 10 mm thick, with addition of stone aggregate, brick chips, and sand. The outer plaster layer on top of it is 10 – 15 mm thick, and it contains additions of sand, silt and a larger amount of brick chips and brick powder. The latter were probably added for moisture protection. In contrast to the lower interior walls, the vault and wall surfaces exhibit only a single layer of plaster containing gravel, sand, silt, brick chips and brick dust with a thickness of 10 – 15 mm. These were then covered with white lime wash and decorated with paintings. Circular medallions with a Medusa head can still be seen on the ceiling. The rear wall was painted with multi-colored fields, lines, plant motifs, birds and a seated figure in niche II. Surface



a)

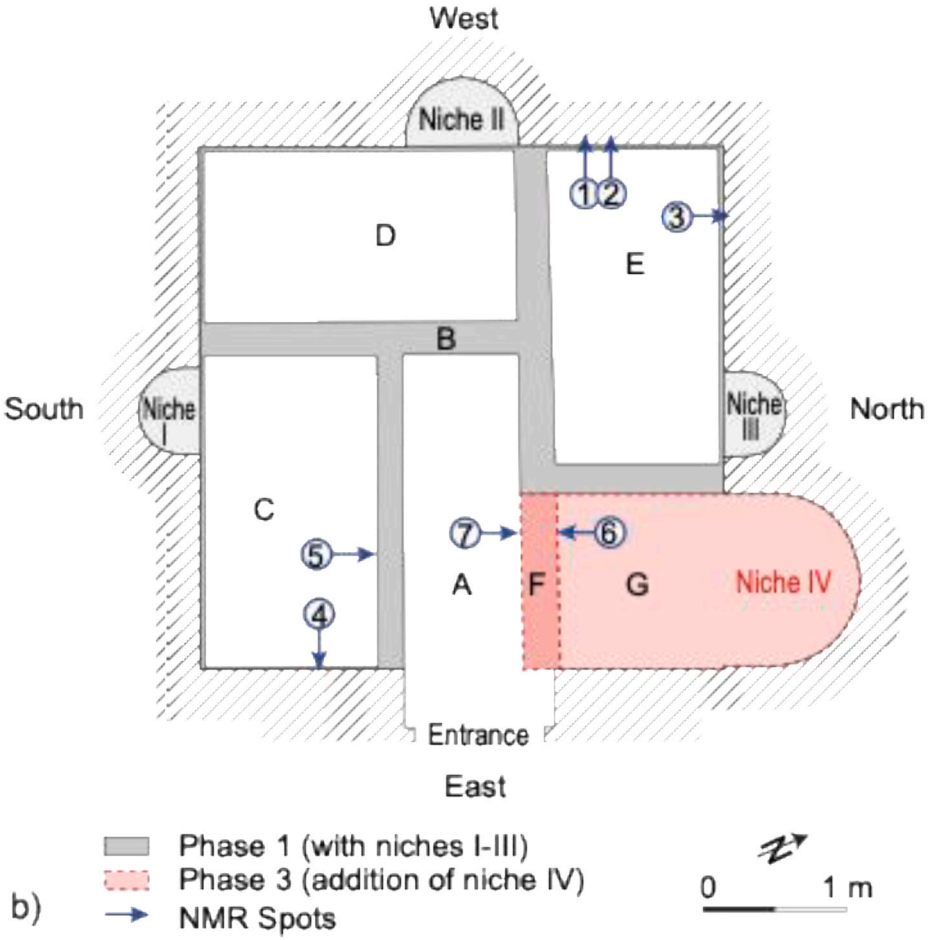

b)

Fig. 1. The Reichertsberg burial chamber. a) View inside from the entrance. b) Floor plan of the chamber. The different building phases and the measurement spots are identified. The phase-1 plasters on the chamber walls and the lower walls dividing the burial sites differ in composition along with the plaster from phase 3.

evaporation of water rising from the soil and pressing from the mountain slope at the foot of the Reichertsberg led to the formation of a 0.2–0.3 mm thick, glaze-transparent sinter crust on top of the paint layer. Over the years the moisture flux caused parts of the ceiling plaster to collapse.

In phase 2, the partially fallen plaster of the vault had to be renewed. The up to 15 mm thick single-layer renovation plaster was only applied to damaged sections of the vault and showed almost no brick chips. On a white coating, a new circular medallion with Medusa's head and a wreath of leaves and flowers were painted. The west wall remained intact and was not painted over. If the east wall was also renovated was not specified in 1998 [3].

In phase 3, an additional niche (Fig. 1b, niche IV) was built into the north-east corner of the chamber, and a small internal wall (Fig. 1b–F) was erected to create another burial compartment (Fig. 1b–G). This brick wall had a 10 – 15 mm thick brownish plaster base coat. An outer 10 –15 mm thick plaster coat was applied on top of it. The niche was also covered with two layers of plaster, which differ from the interior wall in terms of the composition of the aggregates, even though both originate from the same phase.

In phase 4, two sandstone sarcophagi for two individuals were placed on top of the interior walls. The sarcophagi were removed in 1998 and are now on display in the lobby of the school.

In post-Roman times, the chamber gradually filled with mud from the Reichertsberg mountain. During the excavation in 1967, the clay crust was not completely removed from the walls to protect the paintings, which makes it difficult to assess the paintings today. Since the plaster layers from the first phase were partially covered by the ancient renovation and the post-Roman clay crust, the thickness of the plaster layers could only partly be estimated in the non-invasive investigation in 1998 [3]. Therefore, the aim of the NMR depth profiling study was to differentiate the plaster layers from the side walls and the section walls with reference to the building phases 1 to 3 (Fig. 1b).

1.2. NMR depth profiling

NMR depth profiling is a modality of nuclear magnetic resonance (NMR) [4], whereby the relaxation of nuclear magnetization is measured in a sensitive volume located outside the instrument in the inhomogeneous stray-fields of a magnet and a radio frequency (RF) coil by which the magnetization is generated. The sensitive volume has the shape of a thin flat slice, which is aligned parallel to the wall. The magnet with the RF coil is mounted on a precision displacement stage by means of which the sensitive slice can be translated in discrete steps along the depth direction inside the wall to acquire NMR signal at each position. This signal contains essentially the same information as a pixel in a magnetic resonance image (MRI) acquired for the purpose of medical diagnostics with MRI machines in a clinical setting. The basic information is the signal amplitude corresponding to the concentration of NMR-active nuclei, usually hydrogen nuclei in the sensitive slice and the decay time or relaxation time T_2 of the nuclear impulse response to an RF pulse. Either parameter or a combination of them serves as amplitude in a depth profile or one-dimensional image constructed from the manifold of NMR measurements at the different positions of the sensitive slice.

Size and shape of the sensitive slice are defined by the curvatures of the stray fields of the magnet and the RF coil. Both, the magnet and the coil, constitute the stray-field NMR sensor. Different stray-field sensor geometries have been investigated [5–7], but the one most suitable for depth profiling is known as NMR-MOUSE, short for NMR Mobile Universal Surface Explorer [8,9]. The sensor finds various applications in nondestructive materials testing [7,10,11] including the state assessment and conservation treatment of cultural heritage objects [12–16] such as porous stone, paper, easel paintings, mummies, violins, and wall paintings. In the context of the work at stake, investigations of stone conservation treatments [17,18] and stratigraphic analyses of painted walls are of interest, especially depth profiling of Roman frescoes and fresco fragments in Herculaneum [19] and Ostia Antica [20–22] as well as studies of moisture damage of frescoes in Vasari's house in Florence [23] and painted walls in Padua in search for an older, covered wall painting [24].

Such depth profiles reveal the stratigraphy of the plaster layers to which pigments and paint were applied in ancient times. The stratigraphy differs depending on the time of making, the plasters used, and the workshop's craftsmanship [19], and these differences shed light on the status of the building's owner, the use of the room, and the outreach of the plasterer's workshop, and they can assist in sorting and assigning fragments.

To obtain an NMR signal, the plaster layers must contain mobile molecules with hydrogen nuclei. This can be wax from a prior conservation intervention but typically is water. Usually, the wall section to be analyzed is sprayed multiple times with a mist of deionized water prior to depth profiling unless the wall is naturally wet. In the first case the moisture content usually decreases from the surface to the interior of the wall. In the second case, the moisture-concentration gradient may be reversed, and the wall is dryer on the surface than on the inside [25]. From the NMR signal amplitude, the volumetric moisture content $\theta(r)$ can be quantified as a function of depth r inside the wall once the signal amplitude has been referenced to that of pure water. Given the water density ρ, $\theta(r)$ can be converted to water concentration, $\rho\ \theta(r) = c(r)$. Here we approximate the water density at the measurement temperature by 1 g/cm^3.

For purpose of conservation, knowledge of just water concentration is insufficient. The damage to wall paintings arises from the moisture flux, which drags dissolved salts along that solidify on the wall surface upon evaporation of the water. Given the strong gradient G of the magnetic stray field emanating from the NMR-MOUSE magnet into the wall, the moisture flux $J(r)$ inside the wall can be estimated from Fick's first law,

$$J(r) = -D\ \mathrm{d}c(r)/\mathrm{d}r. \quad (1)$$

Here D is the apparent self-diffusion coefficient of the water in the partially saturated porous plaster medium. With knowledge of the magnetic field gradient G it can be determined with the NMR-MOUSE [26], so that it should be possible to estimate the moisture flux nondestructively by means of NMR depth profiling. This nondestructive approach with mobile equipment has not been reported so far with experimental data although moisture flux has been estimated in laboratory studies on samples by NMR [27] and other methods [28]. In the following, the moisture flux in one of the naturally wet, lower dividing walls is reported.

2. Instrumentation and measurement parameters

Depth profiles were measured with a PM25 NMR-MOUSE from Magritek, employing a 15 mm, a 10 mm or no spacer and with a new NMR-MOUSE type sensor developed at the University of Stuttgart [29]. The spacers for the PM25 NMR-MOUSE serve to shorten the distance between the RF coil and the sensitive slice for the benefit of higher sensitivity and at the expense of a reduced depth of access. Without spacers the depth of access corresponding to the maximum length of a depth profile is 25 mm for the PM25 and 12 mm for the new Stuttgart sensor. The dimensions of the sensitive slice are $40 \times 40 \times 0.12$ mm^3 for the PM25 NMR-MOUSE and $\pi \times 20^2 \times 0.12$ mm^3 for the Stuttgart sensor, whereby the thickness of the sensitive slice depends on the acquisition parameters of the measurement (Table 1) [29]. Both sensors were mounted on the same translation stage with the sensors and the translation stage being controlled by a KEA2 console (Magritek, Germany). The console was driven by Magritek's Prospa software installed on a laptop computer with a Windows operating system (Fig. 2). To shield the sensor and the console from external electromagnetic noise, both components were covered with silver-plated parachute silk that was

Table 1
Acquisition parameters for depth profiles.

Spot	1	2	3	4	5	6	7
NMR-MOUSE	PM25	PM25	PM25	PM25	PM25	PM25	Stuttgart
spacer [mm]	15	0	0	10 0	10	10	-
step size [μm]	100	200	200	100 200	200	200	200 200
number of steps	92	131	101	162 132	81	81	26 26
thickness of sensitive slice [μm]	200	120	120	120	120	120	120
number of scans	128	256	256	128 256	128	128	256 256
number of echoes	32	10	10	32 10	32	32	32
echo time [μs]	82	124	124	82 124	82	82	100
90° pulse length [μs]	9	30	30	16 30	16	16	16.5
recycle delay [ms]	200	200	200	300	300	300	300

connected to a common electric ground (Fig. 3, top left).

Depth profiles from the walls were acquired at seven different positions in the burial chamber (Fig. 1b) using CPMG echo sequences with different parameter settings (Table 1) [4]. The spots were selected in consideration of archeological significance, ease of access, and flatness of the wall. The profile value at each depth corresponds to the average amplitude of echoes 2 to 8 in the acquired multi-echo train recorded for each position of the sensitive slice. Averaging the initial echoes increases the signal-to-noise ratio and introduces a relaxation weight. As the relaxation weight did not appreciably change, the signal linearly scales with the moisture content in the depth profiles presented here. To further improve the signal-to-noise ratio, the depth profiles were smoothed with a moving five-point average filter. The profiles at spots 5 and 7 were measured in two runs each covering different depth ranges. At spots 1, 4, 5, and 6, trains of 32 echoes were acquired, long enough for the multi-echo train to decay close to zero so that the relaxation curves can be inverted to distributions of relaxation times to compare the physical properties of the plasters from the different building phases.

The walls were moisturized with multiple sprays of a fine mist of deionized water prior to measurement at all spots but spot 5 which was already known to be naturally wet. Depending on the amount of water sprayed onto the wall, the permeability of the plaster, and the time of measurement the water concentration of these walls varies with depth. At spot 5 the moisture flux inside the naturally wet wall was estimated from the experimental moisture gradient. Each depth-profile measurement took between 40 and 90 min to acquire. At spots 3 and 5 ultrasonic alignment sensors were tested for the first time to assist in the alignment of the sensitive slice parallel to the wall in places where sensor alignment by eye is difficult [25].

3. Results and discussion

3.1. Depth profiles

All profiles but that at spot 7 have been acquired with the PM25 NMR-MOUSE, whereas the spot-7 profile was measured with the newly developed, lighter and more compact Stuttgart sensor with half the depth of access of the PM25 (Fig. 3) [29]. The acquisition parameters are summarized in Table 1. The profiles from spots 4 and spots 7 were measured in two steps to extend the depth range of measurement. In both cases the two profile sections were combined into one after measurement. The two sections for spot 4 were acquired with different parameter settings and combined by matching the hump at 14 mm depth after amplitude scaling. The two sections for spot 7 were measured with the same parameter settings and combined by matching the profile amplitudes. By comparison of the depth profiles, the following features were observed (Fig. 3):

Spot 1: The profile was acquired at a spot where the wall was flat and partially covered with a clay crust on top of the white lime covering the wall plaster. The front (left) of the depth profile exhibits a ca. 1 mm wide peak marking the whitewash. This peak does rise sharply but starts with a lower step attributed to the clay crust. Underneath the whitewash, the depth profile is largely flat, indicating constant water concentration. At

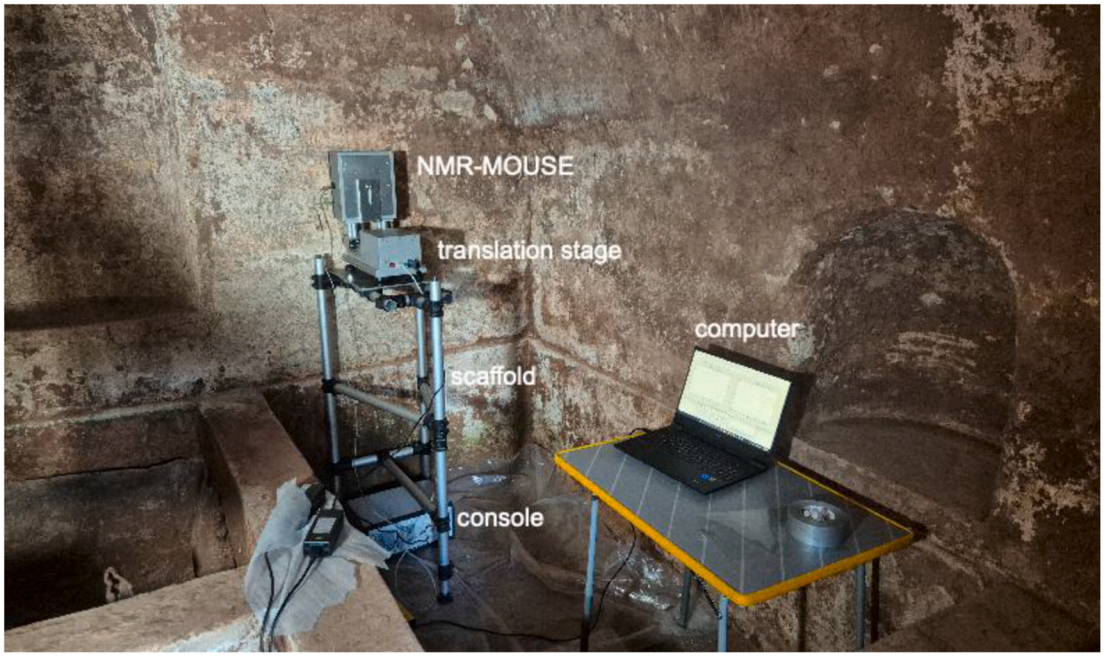

Fig. 2. NMR setup for measuring depth profiles. The NMR-MOUSE is mounted on a precision translation stage, which rests on an adjustable scaffold. The sensor and the translation stage are connected to the console, which is operated by the computer.

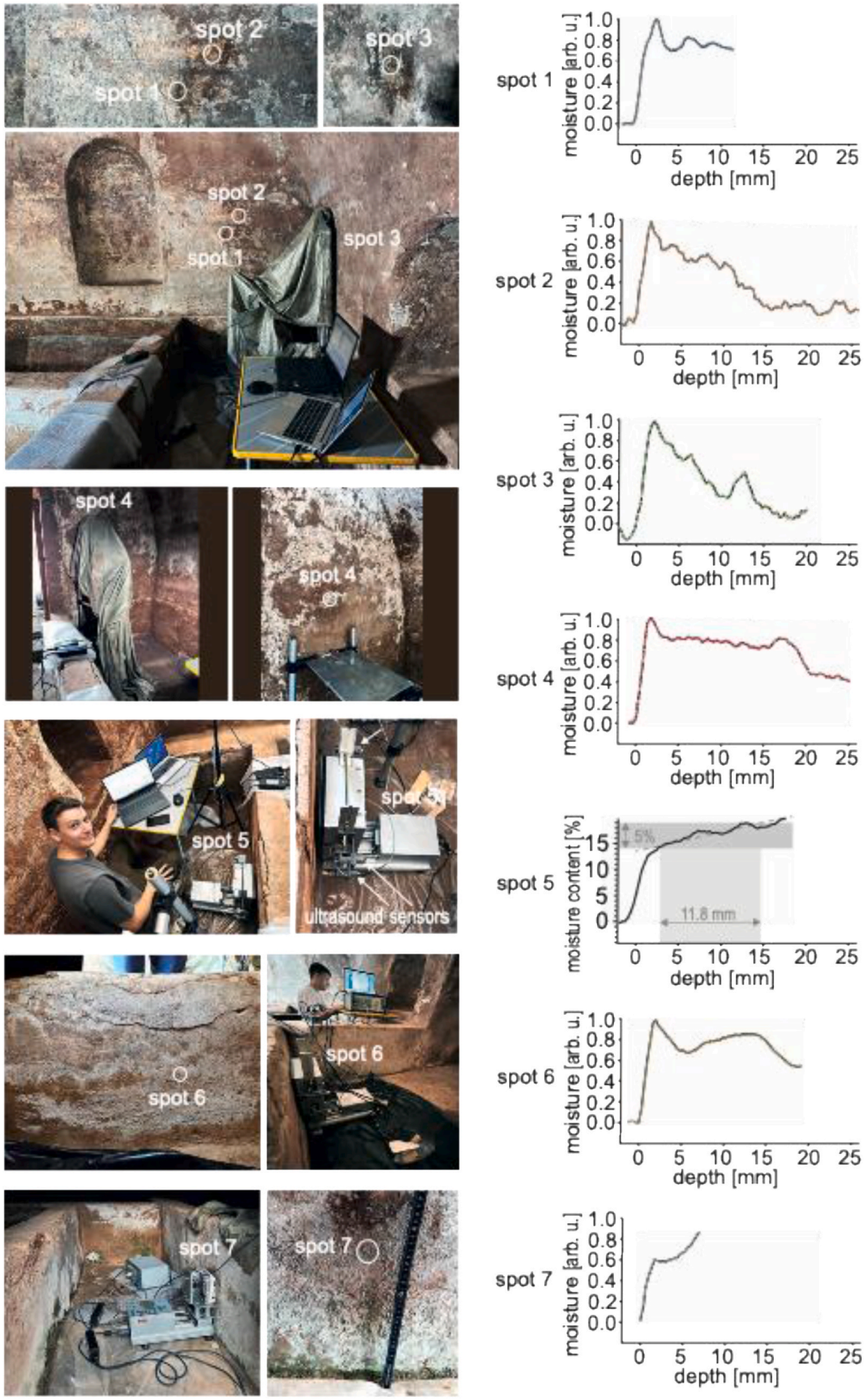

Fig. 3. Details of the measurement spots (left) and the measured depth profiles (right). The locations of the spots are marked in the map of Fig. 1b, and the measurement parameters are summarized in Table 1.

about 4 to 5 mm depth an elevated plateau rises above the noise level, which could not be observed in the other phase-1 depth profiles at spots 2 and 3, so that it is attributed to inhomogeneities from stone aggregate. The profile has been acquired with many scans and a 15 mm spacer for maximum sensitivity along with full echo train decays at each step to allow characterization of the plaster properties by means of depth resolved distributions of relaxation times in comparison with the plasters at spots 4, 5, and 6.

Spots 2 and 3: To assess the thickness of the phase-1 plaster layers, the spacer was removed from the NMR-MOUSE, giving access to the maximum depth range of 25 mm at the expense of measurement sensitivity. Accordingly, the depth profiles are noisy. But despite the measurement noise and the water concentration decreasing with depth, the plaster thickness can be estimated to about 13 mm at both spots.

Spot 4 is located at the east wall of the burial chamber (Fig. 1b), where it is uncertain in how far the plaster has been renewed in phase 2 during renovation. Therefore, to characterize the plaster composition by means of distributions of relaxation times the measurements were conducted with higher signal-to-noise ratio employing a 10 mm spacer, which limits the depth of access to 15 mm. The measurement spot was chosen to be largely free of clay crust. A lime-layer peak is visible in the depth profile at the surface followed by a smooth profile section lacking the aggregate inhomogeneity found at spot 1. Because the profile amplitude appeared to rise at the very end near 14 mm depth it was decided to measure deeper down into the wall the next day after removing the spacer to access the full depth range of the sensor. The profiles from both measurements were subsequently composed into one, whereby the height of the second profile was scaled to match the shape and height of the small elevation at the end of the first profile. Interestingly, another, larger peak reminiscent of but broader than the lime-wash peak at the surface is noted at 18 mm depth followed by a decrease of the profile amplitude at 20 mm to a lower value different from zero. This suggests the existence of a second plaster layer underneath the first one. Comparing the profile from spot 4 to the profiles from spots 1 to 3, it is noted, that all four profiles show the lime-wash peak at the surface, but that the top plaster layer at spot 4 is thicker and more homogeneous than the phase-1 plaster layers from spots 2 and 3.

Spot 5 is at a lower inside wall built during phase 1. It had not been moisturized prior to measurement, because it was naturally wet. The depth profile was measured with a 10 mm spacer and 32 echoes to optimize sensitivity and observe the complete echo-train decays. The profile does not peak at the surface of the wall reporting the lack of a surface layer such as lime wash. With increasing depth, the moisture concentration increases pretty much linearly, indicating rising damp from the ground which is dissipated into the atmosphere through the wall surface. To quantify the moisture flux in the wall, the NMR signal amplitude was normalized to the NMR signal from water in a rubber balloon with the sensitive slice completely inside the water volume. So long as the densities of the pore water and the water in the balloon are identical the normalized signal provides the volumetric water content, which scales from zero for a dry material to the porosity of a fully water saturated porous medium. It is shown on the abscissa of the depth profile for spot 5 in Fig. 3. Approximating the temperature-dependent water density by 1 g/cm^3 the water concentration and its gradient are obtained from the depth profile. Along with the apparent diffusion coefficient, the moisture flux inside the wall towards its surface can be estimated from Fick's first law (vide infra).

Spot 6 is at a wall from the third building phase. The profile amplitude varied considerably but smoothly across depth. While depth profiles of frescoes from Herculaneum or Ostia Antica drawn on a base of multiple plaster layers show sharp transitions between different plaster layers [19,20,22], the smooth variation in moisture concentration observed here suggests, that the moisture profile may result from the combined effect of being naturally wet with moisture moving from the interior to the outside in competition with water moving from the outside to the interior as a result of spraying the wall with a moisture mist prior to measurement. The hypothesis that the wall is naturally wet is corroborated by the depth profile at spot 7 from the other side of the same wall. The signal drop at about 16 mm depth may be the result of partial detachment of the plaster from the wall.

Spot 7: The depth profile has been measured from the outer side of the same phase-3 wall as spot 6 but with the new NMR sensor developed at the University of Stuttgart [29] and not with the PM25 NMR-MOUSE. Due to shorter depth of access, the profile was acquired in two steps with the same acquisition parameters but different positions of the translation stage. The two profiles were subsequently combined by matching the absolute amplitudes of both profile sections. Although the wall had also been sprayed with water prior to measurement, the water concentration rises steeply towards larger depth, indicating that the wall is naturally wet. Interestingly, the moisture gradient appears to be higher than that at spot 5 of the phase-1 wall on the other side of the entrance way. The difference could be explained with a porosity gradient in the plaster layer resulting from higher pressure being applied to the wet plaster when finishing the wall. Due to limited measuring time, the abscissa of the profile had not been calibrated to quantitative volumetric moisture content, and the apparent diffusion coefficient had not been determined.

3.2. Distributions of relaxation times

Distributions of relaxation times were measured for the plasters at spots 1,4,5 and 6 attributed to building phases 1, 1 or 2, and 3 to look for clues on differences in the physical properties of plaster layers relating to wetting behavior and pore size (Fig. 4). While the profile at spot 1 has been acquired with 0.1 mm step size, the step size of the other three profiles was 0.2 mm (Fig. 4, middle). The profiles at spots 1 and 4 are from the inside front and back walls, the other profiles from spots 5 and 6 are from the inner dividing walls. Apart from the high-intensity peaks of the lime layer at the walls the relaxation-time distributions from spots 1 and 4 vary little with depth. Both sets of spatially resolved relaxation-time distributions look similar. The profile from spot 6 also shows a high-intensity peak at the wall surface, but it is broader than the peaks in the profiles from spots 1 and 4 and likely to result from surface degradation due to salt accumulation (salt analyses are reported in Supplement S1). On the other hand, the distributions at spots 5 and 6 vary more strongly with depth and exhibit several regions with high moisture content. The depth-resolved relaxation-time distributions confirm that the plaster composition of the lower dividing walls is different from that of the plaster on the outer walls, whereby the composition of the plaster at spot 6 (phase 3) is more heterogeneous than that at spot 5 (phase 1).

The difference between plasters from spots 5 and 6 is also evidenced in the distributions of relaxation times averaged over the depth range from 3 to 10 mm (Fig. 4, right and left). The exact position of the main peak is different in all four average distributions. But this can be an effect of either plaster composition or moisture concentration [4]. Assuming comparative moisture concentration, then the plaster at spot 1 is also different from the plasters at spots 4 and 6. This is also evidenced by the logarithmic mean relaxation times in the average distributions (red lines in Fig. 4, right and left). Moreover, the small peak at short relaxation time in the average distribution from spot 1 is missing in the average distribution from spot 4, suggesting that both plaster compositions are different, so that the inner front wall may indeed have been repaired in building phase 2.

3.3. Estimation of moisture flux

Spot 5 at one of the inner dividing walls from building phase 1 was known to be naturally moist, and therefore not sprayed with water before measurement of the depth profile (Fig. 3, spot 5). The depth profile shows moisture content increasing with depth, that is, the wall is wetter on the inside than on the outside. The recorded abscissa of the profile reports the average amplitude of echoes 2 to 8 from the measured echo train. Given that the echo trains decayed into the noise after 32

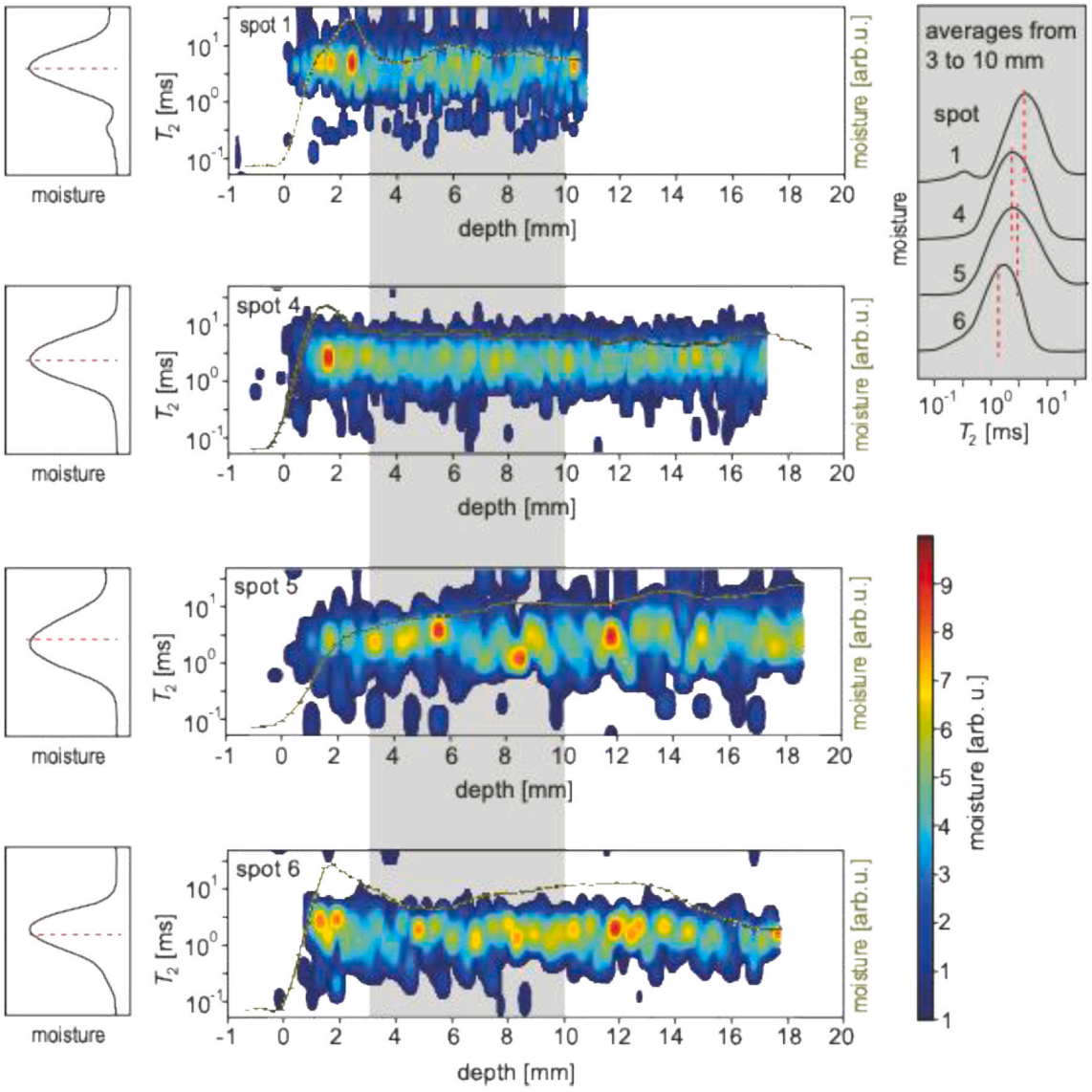

Fig. 4. Distributions of relaxation times for plasters from different building phases. Top to bottom: Spot 1, phase 1; spot 4, phase 1 or 2; spot 5, phase 1; spot 6, phase 3. Left and right: Distribution averages from 3 to 10 mm depth. The logarithmic mean T_2 is marked by a dashed red line. Middle: Depth-resolved relaxation-time distributions with superimposed moisture-content profiles from Fig. 3. (For interpretation of the references to color in this figure legend, the reader is referred to the Web version of this article.)

echoes, the relaxation weight of the average echo amplitude is estimated to 0.7. Scaling the average echo amplitude with this value and normalizing it to the echo amplitude of pure water measured with the same parameters as the depth profile yields the water content θ on the profile ordinate (Fig. 3, spot 5) with an average gradient of $d\theta(r)/dr = (0.05\ m^3/m^3)/(0.0118\ m) = 4.237\ m^{-1}$.

Inserting this value into Fick's first law (1) along with the water density $\rho = 1\ g/cm^3$, the moisture flux $J(r)$ can be estimated, given the apparent diffusion coefficient D which has been determined from the diffusive NMR signal decay measured with the stimulated echo sequence [26] using the parameters listed in Table 2 as $D = (7 \pm 2)\ 10^{-9}\ m^2/s$ (Fig. 5). Accounting for the negative sign of the gradient, the moisture flux towards the wall surface is $J(r) \approx 30\ 10^{-6}\ L/(m^2\ s) = 2.6\ L/(m^2\ d)$. This value inside the plaster layer is in the same range as values obtained at the surface of a cement block in an exploratory study of moisture flux through the surface determined gravimetrically and in parallel by NMR. Details are reported in Supplement S2. Note, that the value of D measured in the burial chamber is larger than the self-diffusion coefficient $D_w = 2.3\ 10^{-9}\ m^2/s$ of pure water at 25 °C due to the rapid liquid-vapor exchange of water molecules inside partially filled pores as described by the two-site Kärger exchange model [30]. According to this the diffusivities of liquid water and water vapor collapse into one

Table 2
Parameters for measuring the apparent diffusion coefficient with the stimulated echo sequence at spot 5.

Quantity	Value
NMR-MOUSE	PM25
spacer [mm]	10
gradient	6.576 T/m
δ range [ms]	0.0055 – 0.3
Δ [ms]	1
number of δ points	5
number of scans	1024
number of echoes	48
echo time [μs]	82
recycle delay [ms]	500
90° pulse length [μs]	16

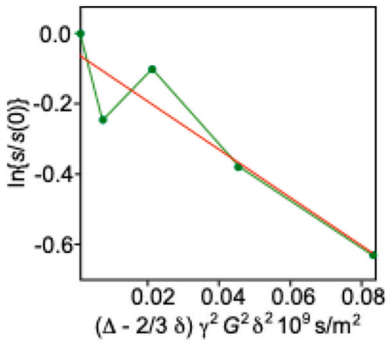

Fig. 5. Diffusive attenuation of the NMR signal *s* (green) and linear fit (red) in a stimulated echo measurement [26]. The slope provides the apparent diffusion coefficient $D = (7 \pm 2)\ 10^{-9}$ m^2/s. (For interpretation of the references to color in this figure legend, the reader is referred to the Web version of this article.)

population-averaged diffusivity in the fast exchange limit, whereby the diffusivity of water vapor is four orders of magnitude higher than that of liquid water. Given the measured apparent diffusion coefficient, the diffusive length scale is about double the maximum pore diameter reported in the literature for historic Roman cement mortars [31], so that it is reasonable to assume that the experimental parameters (Table 2) probe diffusion close to the tortuosity limit [32].

An equivalent way to express moisture transport is to convert the superficial flux J into the actual average pore-water velocity. Since J represents a Darcy velocity, the mean velocity of water within the liquid-filled pore space is higher by a factor of $1/(\varphi S)$, where φ is the porosity and S the degree of saturation. This relationship between Darcy velocity and the actual seepage velocity within the fluid-filled pore space is well established in porous-media theory [33,34]. Using $\varphi = 0.30$, the average open pore porosity of the mortars from Constantine's Basilica in Trier [35], and a representative saturation $S = 0.5$ calculated from the moisture concentration (Fig. 3) and the porosity, the pore-scale velocity becomes $v_{pore} = J/(\varphi S) \approx 2\ 10^{-7}$ m/s, which corresponds to about 1.7 10^{-2} m/d. This implies that, under these moisture conditions, water would advance through the connected pore network at a rate of almost 2 cm per day.

The wall in question (Fig. 6) has a surface area of 1.36 m^2. To estimate the order of magnitude of moisture volume advancing towards the surface of this wall per day, it is assumed that the moisture gradient is the same near all surfaces of the wall. With the calculated flux, this means that each day 3.5 L of water are transported per day towards the surface of this wall. Clearly this is a crude estimate, considering that some regions of the wall are dryer and that the apparent diffusion coefficient depends on the water saturation. Also, the signal decay by relaxation has been neglected in the evaluation of the apparent diffusion coefficient so that the coefficient may be overestimated. Moreover, this is the flux inside the wall and not necessarily the flux through the wall surface. To determine the latter, the moisture gradient at the surface needs to be known, but the apparent, measured gradient is also impacted by the unevenness of the surface and alignment imperfection of the sensitive slice with the wall (cf. Supplement 2), which can be improved for flat surfaces with the assistance of alignment sensors. The total amount of moisture emanating from the walls inside the burial chamber on the measurement day is likely to be higher than the number estimated from the moisture flux and surface area of this one wall, given that the NMR depth profiles from spots 6 and 7 showed that at least also the opposing inner wall was wet.

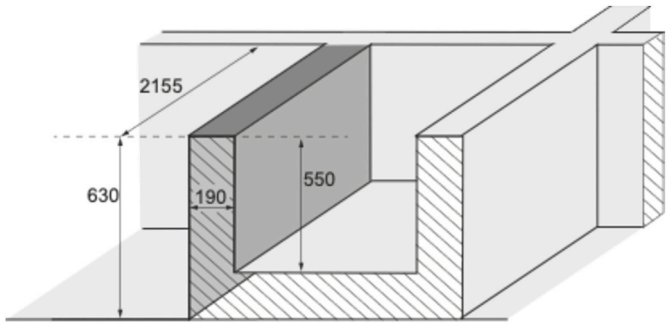

Fig. 6. Dimensions of the wet wall (dark) in millimeters and not drawn to scale. Its surface area is 1.36 m^2.

3.4. Test of alignment sensors

At spots 3 and 5 the parallel alignment of the NMR sensor with the wall was tested for the first time with ultrasonic distance sensors [25]. While at spot 5 the parallel sensor alignment with the wall could be checked by eye, this was more challenging at spot 3 (Fig. 1), given the uneven wall surface and the 214 × 242 mm^2 surface area of the NMR-MOUSE magnet with the 20 × 20 mm^2 coil in the center. Aligning the sensor parallel to the wall is the most critical step in setting up the instrument for measurement of a depth profile, because to maximize the depth range inside the wall, the starting position of the NMR-MOUSE should be as close to the wall as possible (≈1 mm).

To align the NMR-MOUSE with the object plane, four ultrasonic sensors (UM12-1172271, SICK AG, Waldkirch, Germany) were mounted at the corners of the NMR-MOUSE (Fig. 3, spot 5). Each could measure the distance to a wall 100 mm away with a precision of 1 mm. With a minimum distance of 120 mm between the ultrasonic sensors, the smallest misalignment angle from parallel alignment of the sensor and a planar wall that can be measured is 0.27°. This enables depth resolution down to 70 μm with a 40 mm diameter sensitive slice. In view of the uneven surfaces of the burial-chamber walls, the sensors were only crudely calibrated for parallel alignment by visual inspection in the favorable setting of a hotel lobby. To this end, a calibration sample consisting of a 2 mm thick silicone rubber layer between two parallel glass plates (Fig. 7a) was taped onto a flat wall, and depth profiles were measured before and after critical adjustment of the NMR-MOUSE surface parallel to the wall (Fig. 7b). Despite the high noise level attributed to a short measurement-time window, the final profile (Fig. 7b, after) shows a somewhat improved definition of the silicone-rubber contour compared to the initial profile measured before. The sensor readings of this NMR-MOUSE setup were then employed in controlling the sensor alignment during setup of the equipment at spots 3 and 5 in the burial chamber. Whereas to align the NMR-MOUSE with an even surface, three ultrasonic sensors suffice, four sensors proved to be helpful to decide on a compromise for an uneven surface.

4. Summary

The Reichertsberg burial chamber in Trier dates from the 3rd to 4th century of the late Roman Empire. Four building phases were identified

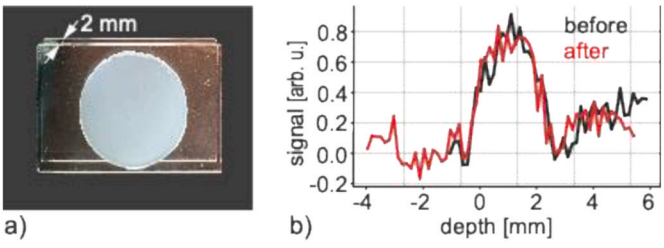

Fig. 7. Calibration of the distance sensors. a) The calibration sample is a 2 mm thick layer of silicone rubber sandwiched between two glass plates. b) Depth profiles before and after visual alignment of the NMR-MOUSE parallel to the glass plates of the calibration sample.

in 1998, during which the inside walls were plastered in phases 1 to 3. Lower, dividing walls encased three burial sites in phase 1, and a fourth burial site was added in phase 3. In phase 2, plaster and paintings on the outer walls were repaired. NMR depth-profiles were measured at seven spots from building phases 1 and 3, whereby it was unknown how many plaster layers were present at spot 4.

The plasters at spots 1 to 4 on the outer chamber walls show a peak at the surface which is attributed to a thin layer of lime wash. The phase-1 plasters at spots 2 and 3 are about 13 mm thick, whereas the plaster at spot 4 is 18 mm thick with a second plaster layer underneath. Depth-resolved relaxation-time distributions of the moisture in the plaster pores confirm that the plaster on the outer chamber walls differs from the plaster on the lower, inner walls (spots 5 and 6) dividing the burial compartments. The physical composition of the plaster on the dividing walls is more heterogeneous than that of the plaster in the chamber walls. Moreover, relaxation time distributions averaged over 7 mm inside the plaster layers also suggest that the plaster at spot 4 is different from the phase-1 plaster at spot 1, supporting the assumption that the wall with spot 4 has been repaired during the renovation phase 2.

Contrary to the chamber walls and the ceiling, the lower dividing walls turned out to be naturally moist. This was obvious for spot 5 with phase-1 plaster, but not for spots 6 and 7 with phase-3 plaster, where the wall moisture was detected only once the depth profiles had been measured. Therefore, spots 6 and 7 had also been sprayed with a mist of deionized water the same way as spots 1 to 4 prior to measurement to enhance the NMR signal from water in the plaster pores giving rise to the initial peaks in the profiles. Spot 5 of the naturally wet wall provided a unique possibility to explore if moisture flux can be measured nondestructively inside moist walls. Following calibration of the volumetric moisture concentration for the spot-5 profile and measurement of the apparent diffusion coefficient, the moisture flux emanating from the wall was estimated from the concentration gradient of the profile and the apparent diffusion coefficient to 2.6 L/(m^2 d). The order of magnitude of this flux has been corroborated in a first laboratory study measuring moisture flux from a model brick under wicking conditions by gravimetry and NMR (cf. Supplement 2). This approach of estimating moisture flux and the limits of the method need to be further substantiated and validated in laboratory studies.

On occasion of the burial-chamber study, also new instrumentation has been tested. One instrument is a stray-field NMR sensor more compact than the PM25 NMR-MOUSE. This new sensor has proven its suitability for depth profiling with the measurement of the spot-7 profile. For field use, it needs to be encased in a robust housing and mounted on a dedicated translation stage. The other instrument comprises a set of ultrasonic distance sensors. These turned out to be helpful in aligning the NMR-MOUSE with the wall in spots where visual sensor positioning is difficult. They will be a crucial asset in future measurements of moisture flux emanating from planar surfaces. While the theoretical alignment precision can exceed 100 μm, the uneven walls of the burial chamber imposed a much larger limit. Nevertheless, the individual readings from the distance sensors helped to optimize the quality of alignment.

Declaration of competing interest

The authors declare that they have no known competing financial interests or personal relationships that could have appeared to influence the work reported in this paper.

Acknowledgements

The measurements were conducted with permission of the Generaldirektion Kulturelles Erbe Rheinland-Pfalz and the Untere Denkmalschutzbehörde (Amt für Stadtkultur und Denkmalschutz, Stadtverwaltung Trier). This work was partially funded by Deutsche Forschungsgemeinschaft (DFG), project number 450272390. Special thanks go to the headmistress of Reichertsberg Elementary School, Ms. Baustert, for allowing the team to work during school hours. The school's caretaker, Mr. Horn, was of great help by providing electricity, appliances, and access.

Appendix A. Supplementary data

Supplementary data to this article can be found online at https://doi.org/10.1016/j.ssnmr.2026.102074.

Data availability

Data will be made available on request.

References

[1] F. Unruh, Trier. Biographie Einer Römischen Stadt, 2017. Von Augusta Treverorum zu Treveris, von Zabern, Darmstadt.
[2] S. Faust, Das "Grutenhäuschen" bei Igel und die Grabkammer am Reichertsberg bei Trier, Trierer Zeitschrift 64 (2001) 143–158.
[3] T. Lutgen, Die spätrömische Grabkammer auf dem Gelände der Grundschule Reichertsberg bei Trier, Trierer Zeitschrift 64 (2001) 159–216.
[4] B. Blümich, S. Haber-Pohlmeier, W. Zia, Compact NMR, DeGruyter, Berlin, 2014.
[5] B. Blümich, C. Rehorn, W. Zia, Magnets for small-scale and portable NMR, in: J. Anders, J. Korvink (Eds.), Micro and Nano Scale NMR, Wiley-VCH, Weinheim, 2018, pp. 1–20, chapter 1.
[6] P. Blümler, F. Casanova, Hardware developments: single-sided magnets, in: M. L. Johns, E.O. Fridjonsson, S.J. Vogt, A. Haber (Eds.), Mobile NMR and MRI, Royal. Soc. Chem., Cambridge, 2015, pp. 110–132, chapter 4.
[7] X. Chen, C. Li, L. Wu, S. Yan, L. Qi, J. Chen, W. Chen, Low-field NMR for polymer science, Giant 24 (2025) 100364.
[8] G. Eidmann, R. Savelsberg, P. Blümler, B. Blümich, The NMR-MOUSE, a Mobile universal surface explorer, J. Magn. Reson. 122 (1996) 104–109.
[9] J. Perlo, F. Casanova, B. Blümich, Profiles with microscopic resolution by single-sided NMR, J. Magn. Reson. 176 (2005) 64–70.
[10] B. Blümich, J. Perlo, F. Casanova, Mobile single-sided NMR, Prog. Nucl. Magn. Reson. Spectrosc. 52 (2008) 197–269.
[11] F. Casanova, J. Perlo, B. Blümich (Eds.), Single-Sided NMR, Springer, Berlin, 2011.
[12] B. Blümich, F. Casanova, J. Perlo, F. Presciutti, C. Anselmi, B. Doherty, Noninvasive testing of art and cultural heritage by Mobile NMR, Accounts Chem. Res. 43 (2010) 761–770.
[13] D. Capitani, V. Di Tullio, N. Proietti, Nuclear Magnetic Resonance to characterize and monitor cultural heritage, Prog. Nucl. Magn. Reson. Spectrosc. 64 (2012) 29–69.
[14] B. Blümich, Concepts and applications of the NMR-MOUSE, in: D.M. Bastidas, E. Cano (Eds.), Advanced Characterization Techniques, Diagnostic Tools and Evaluation Methods in Heritage Science, Springer, Cham, 2018, pp. 61–75.
[15] C. Rehorn, B. Blümich, Cultural Heritage studies with Mobile NMR, Angew. Chem. Int. Ed. 57 (2018) 7304–7312.
[16] NMR in cultural heritage, special issue, in: D. Capitani, N. Proietti (Eds.), Magn. Reson. Chem., vol. 58, 2020 issue 9.
[17] S. Sharma, F. Casanova, W. Wache, A. Segre, B. Blümich, Analysis of historical porous building materials by the NMR-MOUSE, Magn. Reson. Imaging 21 (2003) 249–255.
[18] C. Golini, J. Frick, C. Testa, B. Blümich, J. Anders, L. Brizi, In situ diagnosis of cultural heritage using NMR techniques, Nuovo Cimento Soc. It. Fisica C, Geophys. Space Phys. 48 (2025) 1–4.
[19] C. Rehorn, C. Kehlet, E. Del Federico, W. Zia, T. Meldrum, B. Blümich, Automatizing the comparison of NMR depth profiles, Strain 54 (2018) e1225.
[20] B. Blümich, E.D. Del Federico, D. Jaschtschuk, M. Küppers, K. Fallon, A. Steinfeld, P. Tomassini, Nondestructive analysis of Wall paintings at Ostia Antica, Heritage 4 (2021) 4421–4438.
[21] P. Tomassini, Décorer le port de Rome – la peinture murale d'Ostie, YouTube video, https://www.youtube.com/watch?v=B2X4qULIgQw, last accessed 10 September. 2025.
[22] M. Urbanek, D. Krüger, A. Yong, H. Becker, J. Frick, J. Anders, E. Del Federico, P. Tomassini, B. Blümich, Comparison of wall paintings at Ostia Antica by NMR depth profiling, Heritage Science 12 (2024) 354.
[23] N. Proietti, D. Capitani, R. Lamanna, F. Presciutti, E. Rossi, A.L. Segre, Fresco paintings studied by unilateral NMR, J. Magn. Reson. 177 (2005) 111–117.
[24] V. Tornari, M. Andrianakis, S. Duchêne, et al., A combined ND diagnostic investigation by DHSPI, SIRT, NMR, THZ, on Giotto fresco, J. Cult. Herit. 63 (2023) 206–216.
[25] B. Blümich, J. Anders, When the MOUSE leaves the house, Magnetic Resonance 2 (2021) 149–160.
[26] D.G. Rata, F. Casanova, J. Perlo, D.E. Demco, B. Blümich, Self-diffusion measurements by a mobile single-sided NMR sensor with improved magnetic field gradient, J. Magn. Reson. 180 (2006) 229–235.
[27] L. Pel, K. Kopinga, H. Brocken, Moisture Transport in Porous Building Materials, Heron, 1996, pp. 95–105.

[28] K. Terheiden, Feuchte- Und Salztransport: Charakterisierung Der Interaktion Zwischen Porenfluid Und Porösem Bauwerkstoff, Cuvillier Verlag, Göttingen, 2007 and dissertation, Univ. Weimar, 2007, 9783867274555.pdf.
[29] B.M.K. Alnajjar, J. Frick, B. Blümich, J. Anders, A compact and mobile stray-field NMR sensor, J. Magn. Reson. 369 (2024) 107798.
[30] J. Kärger, Zur Bestimmung der Diffusion in einem Zweibereichsystem mit Hilfe von gepulsten Feldgradienten, Ann. Phys. 479 (1969) 1–4.
[31] A. Klisińska-Kopacz, R. Tišlova, G. Adamski, R. Kozłowski, Pore Structure of historic and repair Roman cement mortars to establish their compatibility, J. Cult. Herit. 4 (2010) 404–410.
[32] P.T. Callaghan, A. Coy, T.P.J. Halperin, K.J. Packer, F.O. Zelaya, Diffusion in porous systems and the influence of the pore morphology in pulsed gradient spin-echo nuclear magnetic resonance studies, J. Chem. Phys. 97 (1992) 651–662.
[33] J. Bear, Dynamics of Fluids in Porous Media, American Elsevier, New York, 1972.
[34] D.A. Nield, A. Bejan, Convection in Porous Media, Springer, New York, 2006.
[35] W. Viöl, K. Krügener, Entwicklung Und Modellhafte Anwendung Nachhaltiger Konservierungsstrategien Für Antropogen Geschädigte, Historische Außenfassaden Sowie Deren Überprüfung Mittels Thz Strahlung am Beispiel Der Konstantinsbasilika in Trier - Bliks, Hochschule HAWK Hildesheim/Holzminden/Göttingen, Fakultät Bauen und Erhalten, 2018.